JOURNAL OF GEOPHYSICAL RESEARCH, VOL. 104, NO. E6, PAGES 14,169–14,178, JUNE 25, 1999

Ganymede's ozone-like absorber: Observations by the Galileo ultraviolet spectrometer

A. R. Hendrix, C. A. Barth, and C. W. Hord

Laboratory for Atmospheric and Space Physics, University of Colorado, Boulder

Abstract. We report on Ultraviolet Spectrometer observations of Ganymede from four orbits of the Galileo primary mission. During 12 observation sequences, regions on Ganymede's leading, trailing, and anti-Jovian hemispheres were observed at several latitudes and varying observational geometries. The measurements show an ozone-like absorber concentrated in the polar regions and near sunrise and sunset at low latitudes, with a clear correlation between ozone abundance and solar zenith angle. The absorption maximum is shifted to the red of the gaseous ozone absorption maximum (near 2600 Å), confirming disk-integrated observations by other researchers. Ganymede's absorber may be ozone trapped in the ice lattice, which we propose is due to charged particle bombardment of the surface. At high Sun (small solar zenith angles), the ozone-like absorber is destroyed. The ozone in the polar regions is likely to be long-lived, on account of the large solar zenith angles.

1. Introduction

We discuss disk-resolved observations of Jupiter's icy moon Ganymede by the Galileo ultraviolet spectrometer (UVS). The data reveal a complicated distribution of an ultraviolet absorber on Ganymede, which may be related to its newly discovered magnetosphere [*Kivelson et al*, 1996] and to the oxygen chemistry that occurs in the icy matrix of the surface due to photolysis. We first discuss what is already known about Ganymede's surface from spacecraft and ground-based observations.

Early ground-based measurements showed that Ganymede displays a hemispheric albedo dichotomy, where its trailing hemisphere (centered on 270° W, where 0° W longitude always faces Jupiter) is darker than its leading hemisphere (centered on 90° W) [*Millis and Thompson*, 1975]. The albedo dichotomy has been attributed to enhanced bombardment by Jupiter's corotating magnetosphere on the trailing hemisphere. An additional leading/trailing difference was noted by the International Ultraviolet Explorer (IUE) [*Nelson et al.*, 1987]: Ganymede's trailing hemisphere was found to have an absorber centered shortward of 2800 Å. This absorption feature was noted to be different from Europa's trailing hemisphere absorber, which is centered near 2800 Å and is thought to be due to implantation of sulfur from the magnetosphere interacting with the surface water ice [*Lane et al.*, 1981; *Noll et al*, 1995; *Hendrix et al.*, 1998], creating an SO_2-like absorption. *Nelson et al.* [1987] suggested that an absorber in addition to SO_2 is present on Ganymede's trailing hemisphere; they suggested ozone, caused by magnetospheric oxygen ions being implanted into the icy surface.

The arrival of the Galileo spacecraft has revealed that Ganymede is even more complicated than Earth-based observations have shown. A magnetosphere has been discovered using the magnetometer on board Galileo [*Kivelson et al.*, 1996; *Gurnett et al.*, 1996]. Field lines at Ganymede's polar regions are open to Jupiter's magnetospheric plasma, while closed field lines, covering ~±30°-45° in latitude, shield the equatorial regions. Polar caps on Ganymede, extending down to latitudes of 40°-45°, were discovered by the Voyager spacecraft [*Smith et al.*, 1979]; the Galileo Near-Infrared Mapping Spectrometer (NIMS) found that while water ice is present all over Ganymede's surface, there is less ice in the equatorial regions, and the water ice in the polar regions is finer grained [*Carlson et al.*, 1996].

Features at 5773 Å and 6275 Å were detected on Ganymede's trailing hemisphere in ground-based measurements and attributed to electronic transitions in pairs of oxygen molecules [*Spencer et al.*, 1995; *Calvin et al.*, 1995]. The bombardment by corotating magnetospheric plasma is likely the source of the molecular oxygen [*Reimann et al.*, 1984], on the basis of the longitudinal variation in the absorption band depth [*Calvin et al.*, 1996]. Condensed pure oxygen is not stable at Ganymede's temperatures, so it was suggested that the oxygen is trapped within the surface ice (defect trapping or adsorption) [*Calvin et al.*, 1996]. Additional spectra from the Hubble Space Telescope (HST) Faint Object Spectrograph (FOS) and images from the Wide Field Planetary Camera (WFPC) showed that the oxygen absorption is concentrated at low latitudes [*Calvin and Spencer*, 1997].

Later measurements by the HST FOS [*Noll et al.*, 1996] identified ozone on Ganymede's trailing hemisphere relative to the leading hemisphere. They indicate that the cross section of Ganymede's ozone is broadened and shifted somewhat from gaseous room-temperature ozone, as it is present in the surface ice. The molecular oxygen and ozone are likely related. *Johnson and Jesser* [1997] describe a process by which O_2 and O_3 "microatmospheres" are formed when magnetospheric ions impact and destroy the surface, creating a void or bubble, where a small O_2 atmosphere forms. Ozone may also form in these bubbles through photolysis, and it was suggested that photolysis is a source of the ozone on Ganymede [*Noll et al.*, 1995]. Possibly connected to the charged-particle -induced

Paper number 1999JE900001.
0148-0227/99/1999JE900001$09.00

oxygen chemistry is the discovery of hydrogen atoms escaping from Ganymede's surface, as detected by the Galileo UVS [*Barth et al.*, 1997]. *Barth et al.* [1997] also suggested that UV irradiation of water ice may be the source of the escaping hydrogen and the oxygen chemistry.

An alternative to having molecular oxygen in ice bubbles was proposed by *Vidal et al.* [1997] and *Baragiola and Bahr* [1998], who performed experiments to replicate the visible wavelength oxygen features seen by *Calvin and Spencer* [1997]. They found that the condensed molecular oxygen on Ganymede's surface must exist in regions at temperatures much lower than reported Ganymede surface temperatures, such as in permanently shadowed regions, cracks in the ice, or high-albedo locations.

A connection between the newly discovered magnetosphere and Ganymede's polar caps was suggested by *Johnson* [1997], who thought they might be due to charged-particle bombardment. In addition, *Pappalardo et al.* [1998] find that the open field line regions correspond with the polar caps of Ganymede. Thermal segregation has also been suggested as a source of the caps [*Purves and Pilcher*, 1980], although this idea was challenged by *Hillier et al* [1996] through photometric analysis. *Sieveka and Johnson* [1982] suggested that a combination of sputtering and thermal processing forms the polar caps; they noted that on the trailing hemisphere, darker presumably as a result of charged particle bombardment, the cap boundary is at a higher latitude than on the brighter leading hemisphere. This may be because frost formation is inhibited in darker regions.

In this work, we use additional UVS measurements to explore further the processes occurring at Ganymede's surface, especially those that may affect oxygen chemistry, to understand the distribution of O_2 and O_3 on Ganymede's surface.

2. Observations

The Galileo ultraviolet spectrometer was built at the University of Colorado's Laboratory for Atmospheric and Space Physics and was described by *Hord et al.* [1992]. The observations discussed in this paper were performed using the F channel of the UVS, which covers the 1616 - 3231 Å wavelength range. The calibration is described in *Hendrix* [1996]. The observations were performed in "full-scan" mode, where the grating was stepped over the 528 channels covering the wavelength range in 4.33 s, with 0.006 s integration time at each channel.

These observations were performed during the primary mission of Galileo, between June 1996 and November 1997; they cover a variety of terrain types and latitudes and longitudes on Ganymede, at several spatial resolutions. Plate 1 shows an image of Ganymede from Galileo/Voyager and depicts the regions covered during each observation sequence. Table 1 describes each observation sequence, including the approximate latitude and longitude covered during the observation. In this paper we deal primarily with the higher resolution observations but use the lower resolution observations (GLOBAL) to supplement our higher resolution results. Plate 1 shows the size of one field of view (FOV) during the GLOBAL sequence, near 0° N, 140° W (this is the "standard" region discussed later). The central locations of the other FOVs during the GLOBAL sequence are shown in Table 1.

3. Photometric Corrections

The initial step in the analysis of the UVS Ganymede spectra was to determine the measured reflectance. This was done by averaging 14 spectra (60.67 s total). The average background radiation noise was subtracted from the resultant spectrum, which was then divided by the calibration curve and by a solar spectrum. The solar spectrum used was measured by the Solar-Stellar Irradiance Comparison Experiment (SOLSTICE) [*Rottman et al.*, 1993] and was double boxcar smoothed to match the UVS spectral resolution.

The first step in correcting for photometric variations in brightness was to understand how Ganymede's UV reflectance varies with phase angle. We divided all UVS observations of Ganymede (both disk-resolved and disk-integrated) into leading (0° - 180° W) and trailing (180° - 360° W) hemisphere data. Including UVS data not discussed in this paper, we used a phase angle range of 10.4° - 81.8° for the leading hemisphere, and a phase angle range of 1.3°-86.7° for the trailing hemisphere. We found that the single-lobed Henyey-Greenstein phase function [*Hapke*, 1993] with an asymmetry parameter of g=-0.35 adequately fits the UVS Ganymede data at all wavelengths in both longitude bins. However, the phase curve is not a perfect fit; this is because individual terrain types behave differently photometrically. In spite of this, we use this simple phase curve for all observed regions, aware

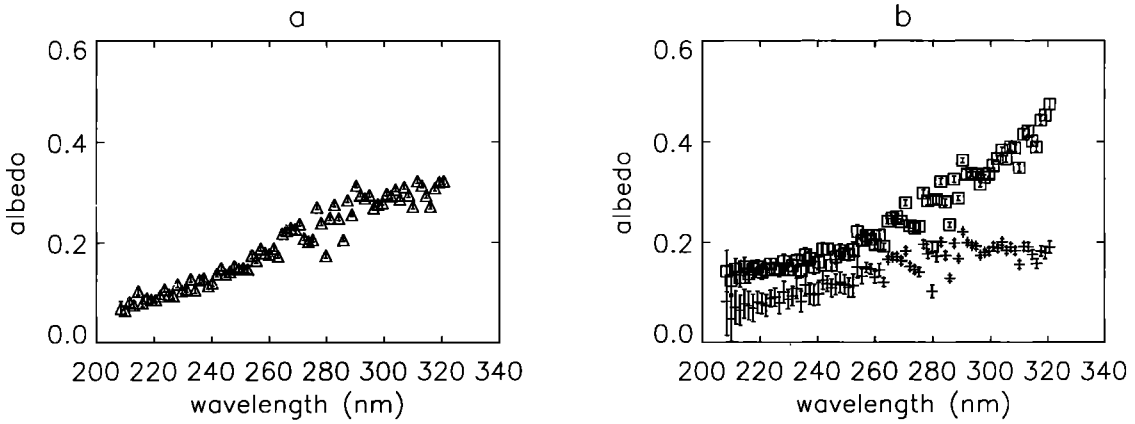

Figure 1. Albedos from three different locations (see Plate 1). (a) Standard region albedo, (b) average albedos from PTAH and DRKLIT regions; DRKLIT albedo has been offset by 0.05 for clarity. Statistical error bars are shown.

that the correction may not be perfect but assuming that the phase curve does not vary significantly with wavelength. Therefore the magnitudes but not the shapes of the derived albedos are affected. In the analysis of the resultant albedos, we focus not on variations in brightness but in variations in albedo with wavelength, which can indicate the presence of absorption features. Ganymede's UV phase curve will be studied further in future work.

The next step in the photometric correction was to solve for the single-scatter albedo $\omega(\lambda)$ of each region using a simplified version of the Hapke photometric function [*Hapke*, 1993, p. 233], where we ignored the opposition effect and multiple scattering. Multiple scattering may be assumed to be negligible at these wavelengths. The opposition effect term at ultraviolet wavelengths is unknown for any terrain type; this will be investigated in a future study. To account for macroscopic surface roughness, we use the terms from *Hapke* [1993, pp. 344-345] with $\overline{\Theta}=32°$, which is consistent with the visible results from *Domingue and Verbiscer* [1997]; the surface roughness parameter is not expected to vary with wavelength. This photometric correction is very simple and is not expected to accurately correct for photometric variations in all observations. However, in this study we are concerned primarily with shapes of albedo ratios (discussed below), which should be unaffected over this short wavelength range by variations in photometric parameters.

4. Results

4.1 Albedos

The method described above was used to determine the albedo of each observed region. Figure 1 displays three of these albedos, binned into 15 Å bins to reduce scatter. The albedos shown are the average albedo measured during three observation sequences, of three different terrains and have distinctly different shapes. The southern polar PTAH region is brighter than the other regions, particularly at longer wavelengths. The albedo of the standard region (described below) is lower than PTAH's and is flatter at longer wavelengths. The DRKLIT albedo, corresponding to a leading hemisphere region, is flatter than the albedos of the other regions. Generally, leading hemisphere regions have albedo that are relatively flat longward of ~2900 Å; this is also seen in UVS spectra of regions on Europa's and Callisto's leading hemispheres. This spectral characteristic will be investigated and discussed in a later report.

4.2 Albedo Ratios

We display the variation in albedo from place to place on the surface by ratioing the albedo of each region to the albedo of a "standard" region (part of the GLOBAL sequence). The albedo of the standard region is shown in Figure 1a. We have chosen this as the standard albedo as it was observed with relatively low spatial resolution, so it is not the albedo of any particular, and possibly anomalous, region; the albedo was measured when the solar and emission angles were approximately equal. Furthermore, the standard region covers an equatorial portion of the leading hemisphere, near 140° W longitude, so it is an appropriate region to which to compare trailing hemisphere and polar data. The albedo ratio of one region (PTAH) to the standard is shown in Figure 2. The ratio indicates that an absorber is present in the PTAH region

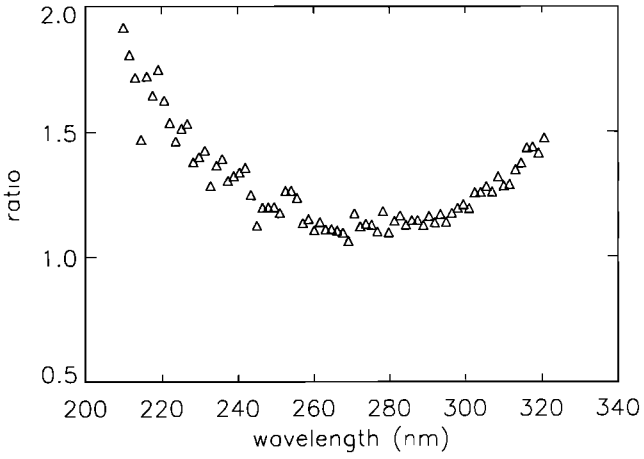

Figure 2. Albedo ratio: PTAH average albedo/standard region albedo.

which is not present in the standard region, and it absorbs between 2600 and 2800 Å.

4.3 Comparisons With Ozone Cross Section

We follow the method of *Noll et al.* [1996] and compare Ganymede's ultraviolet absorption band with ozone, which absorbs strongly near 2600 Å. The cross section of gaseous ozone [*DeMore et al.*, 1994] is shown in Figure 3a. When we shift this cross section 197 Å to the red and broaden the full width at half maximum (FWHM) from ~ 400 Å to ~ 950 Å, which is similar to the FWHM of solid O_3 [*Vaida et al*, 1989], we obtain the "ozone-like" cross section also shown in Figure 3a. For this cross section we have also normalized the magnitude of the absorption maximum to correspond with that of gaseous ozone. As was noted by *Noll et al.* [1996], the shifting and broadening of the O_3 cross section may be caused by the presence of O_3 in water ice.

We note that in deriving the ozone-like cross section, the shift to the red is greater than the shift required to fit the HST data of *Noll et al.* [1996]. This is simply due to the albedo ratio used: *Noll et al.* [1996] ratioed the disk-integrated trailing hemisphere albedo to the disk-integrated leading hemisphere albedo; we are using disk-resolved albedos and have somewhat arbitrarily chosen a leading hemisphere standard region. Using a different leading hemisphere standard region (or a leading hemisphere disk-integrated albedo) would likely result in a different shape for the cross section. This is why we refer to the absorber as "ozone-like": we are utilizing it mainly to quantify the relative amount of absorption across the surface. Laboratory measurements of ozone in ice under Ganymede's conditions are needed to understand absolute quantities of the absorber.

We use this derived cross section in Beer's law to determine the column density of the ozone-like absorber at each observed location. Figure 3b displays the ratio of the PTAH albedo to the standard albedo, along with a model fit to the albedo ratio: model=$A\exp(-\sigma N)$, where A is a constant derived to fit the ratio magnitude, σ is the ozone-like cross section, and N is the column density derived to fit the absorption band; N includes the slant angle to the location of the observation, $1/\mu+1/\mu_0$. For the PTAH region we obtained a best fit column density of 4.7×10^{16} cm^{-2}.

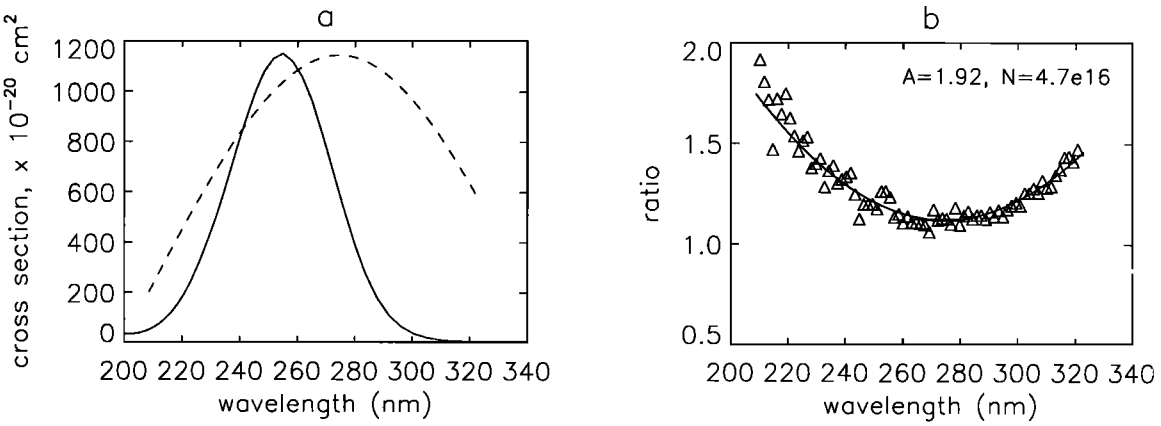

Figure 3. (a) Laboratory-measured cross section of gaseous ozone (solid line) versus ozone-like cross section derived using Galileo UVS Ganymede albedo ratio (dashed line), (b) PTAH/standard albedo ratio compared to model fit with column density N=4.7x10^{16} cm^{-2}.

4.4 Distribution of Ozone-Like Absorber

We investigate the presence and strength of the ozone-like absorption feature at all observed regions on Ganymede. When the albedo of each region is ratioed to the albedo of the standard region, we find that the absorption feature appears to be related, in a complicated way, to both latitude and longitude, with a possible dependence on amount of water ice present as may be indicated by visible brightness of the region. To demonstrate the trends in albedo shape with latitude and longitude, we display a "typical" albedo ratio from each region observed in Figure 4, and explain the features here. When we apply a similar analysis to all observed regions on Ganymede, we find that some regions are fit well by this

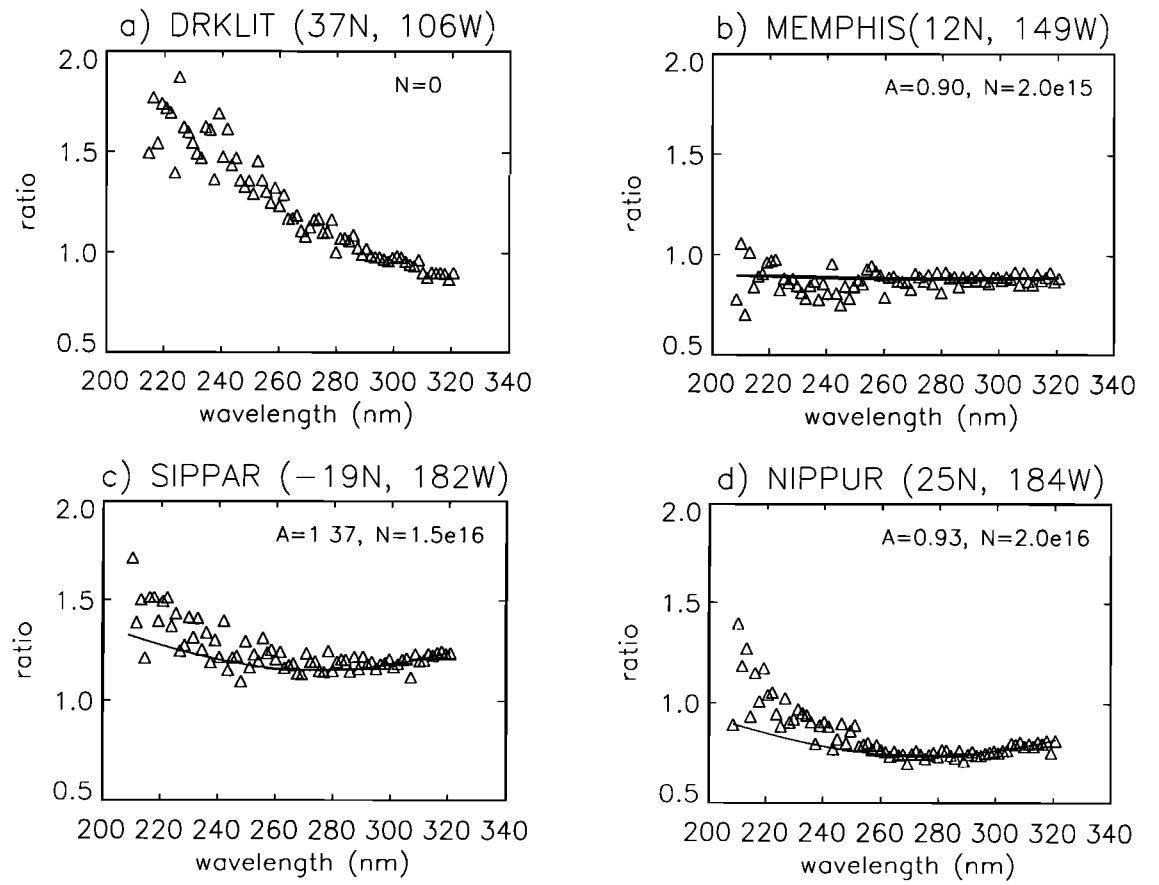

Figure 4. Albedo ratios from several different regions to show how the absorption feature is distributed across the surface. Also shown is the model fit to the albedo ratio, indicating the best fit parameters (N is column density in cm^{-2}) in the model, where model=A exp(-σN). (a) DRKLIT region, (b) MEMPHIS region, (c) SIPPAR region, (d) NIPPUR region, (e) NORTH POLE region, (f) NORTH POLE region, (g) TAMMUZ region, (h) AMON region, (i) NORTH POLE region, (j) NORTH POLE region, (k) BRITRL region, (l) HILAT region.

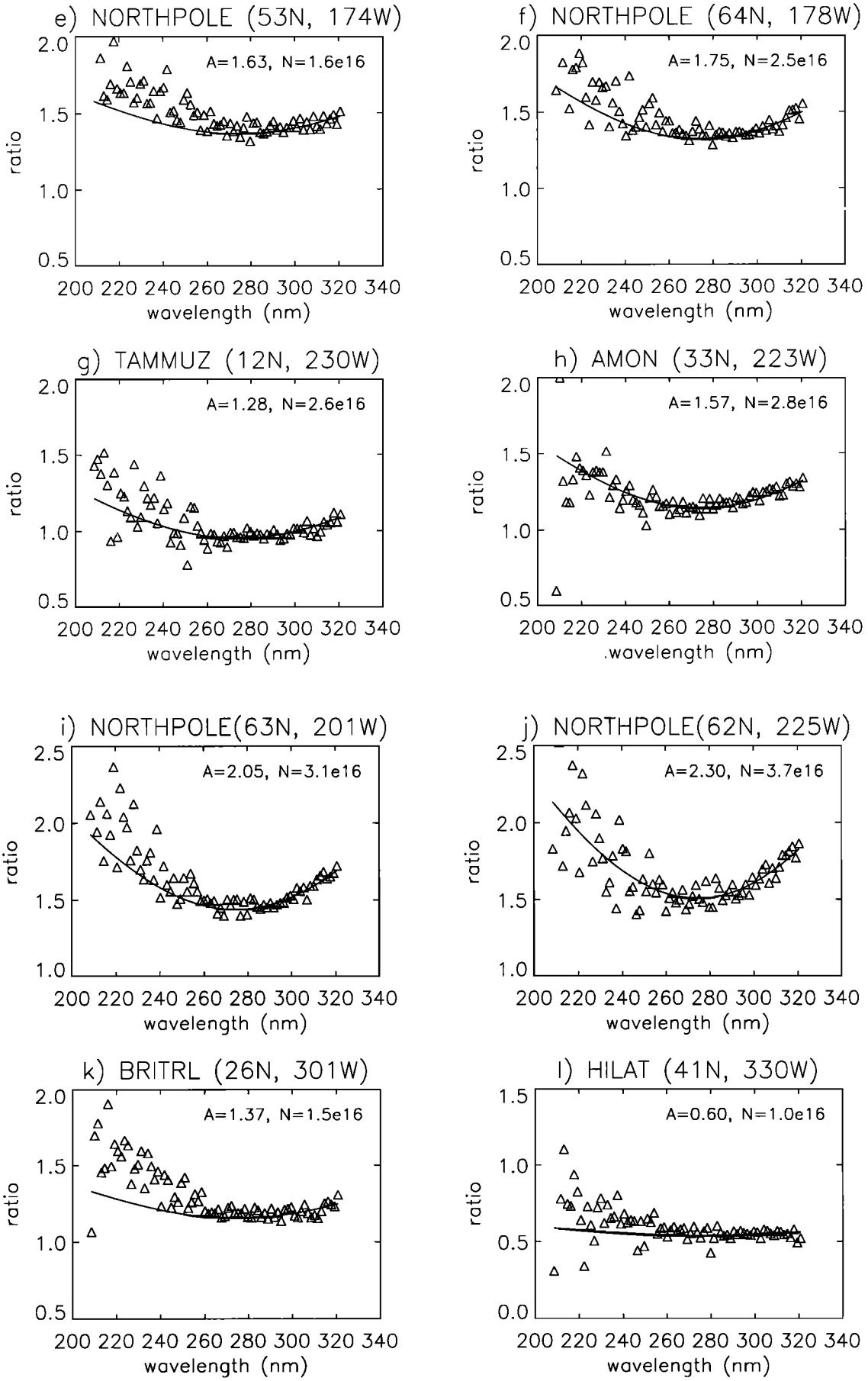

Figure 4. (continued)

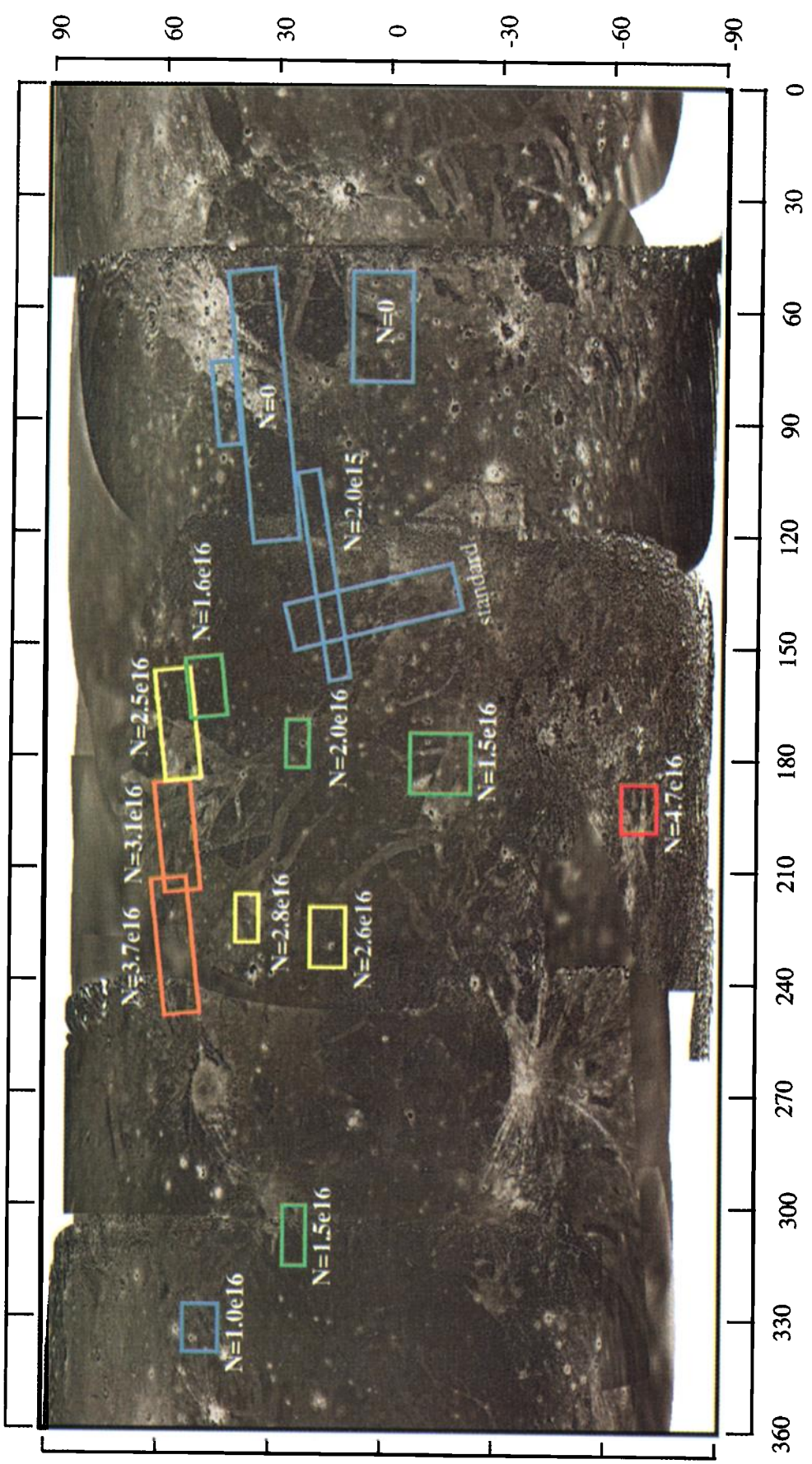

Plate 1. SSI/Voyager global mosaic of Ganymede (courtesy of T. Rosanova and SSI Team) with regions observed by UVS.

ozone-like cross section, with varying column densities, and some are not. Model fits are shown compared to albedo ratios from each observed region in Figure 5. Plate 1 displays the column densities mapped out on a Galileo/Voyager image of Ganymede. Table 1 also displays the best fit column density of the ozone-like absorption for the average albedo of each observed region.

On the leading hemisphere (east of ~120° W), where the DRKLIT and BRILED observation sequences were performed, the albedo ratios (Figure 4a) are generally blue, both at high and middle latitudes; the highest latitude observed in this longitude range is 37° N. The blue albedo ratio indicates that no ozone exists in these locations.

The MEMPHIS region (middle latitudes near 120°-150° W) shows no absorption, making the albedo ratio flat (Figure 4b). This is also where the standard region is, although the MEMPHIS observation was performed with a higher spatial resolution.

Near 180°W, the absorption feature is present in small amounts at low latitudes (SIPPAR and NIPPUR observations, Figures 4c and 4d); at higher latitudes the amount of the absorber varies (NORTH POLE observations, Figures 4e and 4f). Moving slightly closer toward the central trailing hemisphere, the PTAH region (190°-200°W) at high southern latitudes shows the highest quantities of the absorber, as shown in Figure 3b.

In the 200 -240°W longitude region, the lower latitudes (TAMMUZ observation, Figure 4g) show the absorption more strongly than at similar latitudes near 180°W; the higher latitudes (AMON observation, Figure 4h) have an even stronger absorption, while the high northern latitudes (NORTH POLE observations, Figure 4i and 4j) show a very strong absorption.

At middle latitudes near the central trailing hemisphere (BRITRL observation, Figure 4k), the absorber is present in moderate quantities (not as much as in the 180°-240° W region). At higher latitudes near 330°W (HILAT observation, Figure 4l), the absorption feature is not very strong.

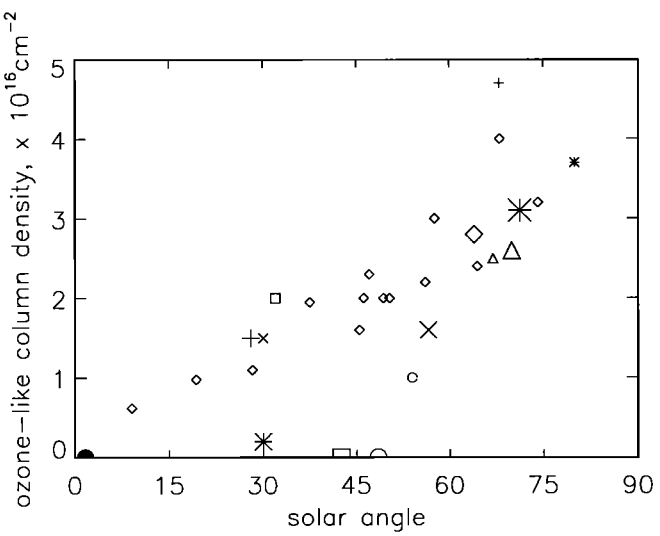

Figure 5. Ozone-like column density versus solar zenith angle. Small diamonds and solid circle, GLOBAL; small plus, PTAH; large cross, small and large asterisks, and small triangle, NORTH POLE; small circle, HILAT; large diamond, AMON; small square, NIPPUR; large plus, BRITRL; large triangle, TAMMUZ; small cross, SIPPAR; large circle, DRKLIT; large square, BRILED; medium asterisk, MEMPHIS.

4.5 Variations in Ozone-Like Absorber with Solar Angle

The derived column densities shown in Figure 4, while not strongly related to latitude or longitude, do have a distinct correlation with solar zenith angle. The ozone-like column density increases with solar zenith angle. In Figure 5 we show the derived ozone-like column density versus solar zenith angle (angle to the Sun measured from the normal). The 29 points in Figure 5 correspond with the observations shown in Plate 1 and Table 1. The ozone-solar angle relationship is particularly strong in the 150°-240° W longitude range, where the most UVS observations exist. The two trailing hemisphere (large plus and small open circle) observations also follow the trend. The leading hemisphere locations (large square, large open circle, and large asterisk) show negligible amounts of ozone despite solar zenith angle being large. We thus detect a strong relationship between solar zenith angle and derived ozone-like column density; this relationship is clear on the anti-Jovian and trailing regions, in contrast to the leading hemisphere, where no ozone-like absorber is measured.

5. Discussion

The UVS results clearly show a relationship between derived ozone-like column density and solar angle, suggesting that the ozone is destroyed by photolysis:

$$O_3 + h\nu \rightarrow O_2 + O(^1D). \quad (1)$$

The creation of the ozone-like absorber at Ganymede is less clear. It is likely that the ozone is related to the molecular oxygen detected by *Calvin and Spencer* [1997]; we speculate here on the possible creation mechanisms of this oxygen chemistry.

A possible source of both the ozone and the molecular oxygen is charged particle bombardment [*Noll et al.*, 1996; *Calvin and Spencer*, 1997; *Johnson*, 1998.]. The evidence for this is that the ozone-like absorber appears more on the trailing hemisphere than on the leading hemisphere, as displayed through the albedo ratios, where the standard albedo is a leading hemisphere region. Other leading hemisphere regions do not display the absorption feature. This leading-trailing asymmetry in ozone was first detected by *Noll et al.* [1996]. Other evidence for bombardment by the corotating plasma is the molecular oxygen found on the trailing hemisphere [*Calvin and Spencer*, 1997], as well as Ganymede's albedo dichotomy, where its trailing hemisphere is darker than its leading hemisphere [*Millis and Thompson*, 1975].

Charged particle bombardment of water ice produces H, OH, O, H_2, O_2, and H [*Johnson*, 1998]; this was discussed as a possible source of the escaping atomic hydrogen detected at Ganymede [*Barth et al.*, 1997]. It has been suggested that the O_2 exists in the ice lattice, where bombardment produces defects in the ice, and movement of the defects (annealing) forms larger bubbles in which O_2 can accumulate (from oxygen atoms) [*Johnson and Quickenden*, 1997]. At low temperatures, molecular oxygen not only is formed less efficiently, but small voids (bubbles) are created, producing a scattering surface. Therefore the lack of annealing at high latitudes results in shorter photon path lengths, so the weak O_2 absorption bands

Table 1. Disk-Resolved Observations

Sequence	Longitude *	Latitude *	Phase Angle, deg.	Solar Zenith Angle, deg.	Number of Observations +	Derived Column Density, cm^{-2}
GLOBAL ++	140° W	0° N	29	13	1	none
	152° W	0° N	29	1	1	none
	162° W	5° S	29	9	1	6 2e15
	171° W	8° S	29	19	1	9 8e15
	180° W	11° S	29	28	1	1.0e16
	189° W	13° S	29	37	1	1.9e16
	199° W	16° S	29	47	1	2.3e16
	210° W	18° S	29	57	1	3.0e16
	220° W	20° S	29	68	1	4.0e16
	151°W	48° N	29	49	1	2.0e16
	169° W	41° N	29	45	1	1.6e16
	180° W	37° N	29	46	1	2.0e16
	191° W	33° N	29	50	1	2.0e16
	202° W	29° N	29	56	1	2.1e16
	213° W	27° N	29	65	1	2.4e16
	225° W	24° N	29	74	1	3.2e16
ISIS-PTAH	190° - 201° W	67° S	24	68	4	4.7e16
NIPPUR	175°-185° W	25°-29° N	25	32	10	2.0e16
MEMPHIS	116° -162° W	9°-22° N	29	12°-52	8	2.0e15
AMON	220° 227° W	32°-34° N	24	64	5	2 8e16
NRPOLE	157°-244° W	54°-66° N	29°-32	57°-84	19	1 6-3 7e16
TAMMUZ	227°-238° W	13° N	26	66°-77	9	2.6e16
SIPPAR	176°-191° W	8°-19° S	31	25°-37	11	1.5e16
DRKLIT	51°-136° W	26°-38° N	10°-19	26°-71	25	none
BRILED	68°-85° W	0°-13° S	22°-25	34°-51	11	none
BRITRL	296°-305° W	26° N	73	28	5	1.5e16
HILAT	327°-333° W	41° N	64	54	3	1.0e16

*Latitude and longitude ranges are for entire observation sequence for all observations except GLOBAL; for GLOBAL, geometries shown are for individual observations within the sequence, and latitude and longitude shown are the FOV boresight latitude and longitude.
+Each observation is an average of 14 spectra
++ The GLOBAL observation centered at 0° N, 140°W, was used as the "standard" region in this study, to which other regions were compared.

are not seen easily. An alternative to O_2 accumulating in bubbles in the ice was suggested by *Baragiola and Bahr* [1998], who find that the O_2 must exist only in very cold regions of Ganymede's surface, such as in cracks or other regions not exposed to sunlight.

Like the molecular oxygen at Ganymede's surface, the ozone is probably created by charged particle bombardment. However, charged particles are unlikely to produce ozone directly. Rather, O_2 accumulates in the ice, and subsequent radiolysis produces ozone [*Johnson and Quickenden,* 1997]. Laboratory experiments have shown that the ozone-like absorption seen at Ganymede by the UVS can be reproduced. R. Baragiola (personal communication, 1998) bombarded an O_2 + H_2O ice mixture with 100 keV H^+ ions and found the ozone-like absorption feature in the laboratory reflectance spectrum. This suggests that charged particle bombardment of Ganymede's trailing hemisphere produces O_2 in the ice; further bombardment produces O_3 in the ice.

Complicating matters of charged particle bombardment is the fact that Ganymede does have its own magnetosphere, which shields the low-latitude surface from some particles [*Kivelson et al.,* 1996]. Particles that are energetic enough to cross the closed field lines include S^+ (of at least 400 keV) and O^+ (of at least 800 keV) (J. Cooper, personal communication,

1998) and make up a significant portion of the trapped particles at Ganymede's orbit [*Ip et al.*, 1997]. Electrons and protons are not energetic enough to cross Ganymede's closed field lines and are deflected around Ganymede or follow the open field lines into the polar regions. It is difficult to understand Ganymede's hemispheric asymmetries when accounting for this magnetosphere; as was shown by *Pospieszalska and Johnson* [1989] and discussed by *Calvin and Spencer* [1997], the low-energy (cold) ions are thought to be responsible for leading-trailing asymmetries, whereas the high-energy (hot) ions affect both the leading and trailing hemispheres. We do not yet know enough about Ganymede's magnetosphere to fully understand what causes these hemispheric asymmetries. Furthermore, the amount of ice lattice damage due to particles of varying energies is not clear and may affect the amount of O_2 and O_3 formed at high and low latitudes by the particles traveling along the open field lines and the particles crossing the closed field lines. *Calvin and Spencer* [1997] suggested that Ganymede's magnetosphere may not be constant in strength, allowing for hemispheric asymmetries to build up.

Other mechanisms to consider are the roles of solar radiation and sputtering by charged particles. Ultraviolet photons may break up the water ice molecules, producing molecular oxygen and ozone, although the penetration depth is not as great as with ions. A longitudinal variation in molecular oxygen and ozone signatures is not expected if solar radiation were the primary source, unless some other process destroys the oxygen and ozone only on the leading hemisphere. Possible methods of destruction of leading hemisphere oxygen and ozone include micrometeorite bombardment [*Calvin and Spencer*, 1997] and sputtering.

Thus our hypothesis is that molecular oxygen (detected by *Calvin and Spencer* [1997]) and ozone are created in the ice by charged particle bombardment. At small solar zenith angles, the ozone is destroyed by photolysis and is reconverted into O_2 and O; at large solar zenith angles and at night, the O_2 and O combine to form O_3. At the poles the solar zenith angle does not become small enough to destroy ozone, so the polar ozone is long-lived.

This hypothesis is supported by the fact that no ozone is detected on the leading hemisphere, nor was molecular oxygen found on the leading hemisphere [*Spencer et al.*, 1995]. This suggests that charged particle bombardment, constrained to the trailing hemisphere longitudes, creates the ozone in the ice. However, if corotating charged particles come into contact with Ganymede's surface through open field lines, we expect to see their signature at all high latitudes, not only on the trailing hemisphere. UVS observations of high latitudes on the leading hemisphere do not exist to confirm whether or not ozone is present there. Furthermore, more needs to be learned about Ganymede's magnetic field before the oxygen chemistry can be fully understood.

6. Conclusions

The Galileo UVS has detected an ozone-like absorption on Ganymede, whose distribution is related to longitude, latitude and solar zenith angle. The absorption feature is centered between 2600 and 2800 Å; it is shifted to the red and broadened compared with gaseous ozone and may be the signature of ozone trapped in the ice matrix. Laboratory measurements of O_3 in ice at Ganymede conditions are needed to further understand the feature.

Observations covering primarily the 150°-240° W region indicate variations in the amount of the ozone-like absorber; this distribution is displayed in Plate 1 as well as in Table 1. Figure 5 shows a strong correlation between the derived ozone column density and the solar zenith angle, whereby less ozone is present at small solar zenith angles.

We have proposed a combination of charged particle bombardment and photolysis for the creation and destruction of the ozone detected by the UVS. Charged particle bombardment, constrained primarily to Ganymede's trailing hemisphere and polar regions, creates ozone in the ice. At low-latitude regions the ozone is converted by photolysis into molecular and atomic oxygen during the day (particularly at small solar zenith angles); polar ozone is likely long-lived. The ozone column density thus depends on longitude (more is created on the trailing hemisphere where there is more charged particle bombardment), and is inversely correlated with solar angle, where the solar angle is measured from the local normal (more ozone exists at large solar zenith angles: at the poles, and at lower latitudes at night, and early and late in the day).

Acknowledgments. The authors thank R. Baragiola, T. Orlando, B. Pappalardo, and J. Cooper for helpful conversations, T. Rosanova for the SSI image, and B. Knapp for the SOLSTICE spectrum. R. E. Johnson and an anonymous reviewer provided constructive comments.

References

Baragiola, R. A., and D. A. Bahr, Laboratory studies of the optical properties and stability of oxygen on Ganymede, *J. Geophys. Res., 103*, 25,865–25,872, 1998.

Barth, C. A., C. W. Hord, A. I F. Stewart, W. R. Pryor, K. E. Simmons, W. E. McClintock, J. M. Ajello, K. L. Naviaux, and J. J. Aiello, Galileo Ultraviolet Spectrometer observations of atomic hydrogen in the atmosphere of Ganymede, *Geophys. Res. Lett., 24*, 2147-2150, 1997.

Calvin, W. M., and J. R. Spencer, Latitudinal distribution of O_2 on Ganymede: Observations with the Hubble Space Telescope, *Icarus, 130*, 505-516, 1997.

Calvin, W M., R. N. Clark, R. H. Brown, and J. R. Spencer, Spectra of the icy Galilean satellites from 0.2 to 5 μm: A compilation, new observations, and a recent summary, *J. Geophys. Res., 100*, 19,041–19,048, 1995.

Calvin, W. M , R. E. Johnson, J. R. Spencer, O_2 on Ganymede: Spectral characteristics and plasma formation mechanisms, *Geophys. Res. Lett , 23*, 673-676, 1996.

Carlson, R., et al., Near-infrared spectroscopy and spectral mapping of Jupiter and the Galilean satellites: Results from Galileo's initial orbit, *Science, 274*, 385-388, 1996.

DeMore, W. B., S. P. Sander, D. M. Golden, R. F. Hampson, M. J. Kurylo, C. J. Howard, A. R. Ravishankara, C. E. Kolb, and M. J. Molina, Chemical kinetics and photochemical data for use in stratospheric modeling, *JPL Publ. 94-26*, 1994.

Domingue, D. L., and A. Verbiscer, Re-analysis of the solar phase curves of the icy Galilean satellites, *Icarus, 128*, 49-74, 1997.

Gurnett, D. A., W. S. Kurth, A. Roux, S. J. Bolton, and C. F. Kennel, Evidence for a magnetosphere at Ganymede from plasma-wave observations by the Galileo spacecraft, *Nature, 384*, 535-537, 1996.

Hapke, B , *Theory of Reflectance and Emittance Spectroscopy*, Cambridge Univ. Press, New York, 1993.

Hendrix, A. R., The Galileo Ultraviolet Spectrometer: In-flight calibration and ultraviolet albedos of the Moon, Gaspra, Ida and Europa, Ph.D. thesis, Univ. of Colo., Boulder, 1996.

Hendrix, A. R., C. A. Barth, C. W. Hord, A. L. Lane, Europa: Disk-resolved ultraviolet measurements using the Galileo Ultraviolet Spectrometer, *Icarus, 135*, 79-94, 1998.

Hillier, J., P. Helfenstein, and J. Veverka, Latitude variations of the polar caps on Ganymede, *Icarus 124*, 308-317, 1996.

Hord, C. W., et al., Galileo Ultraviolet Spectrometer Experiment, *Space Sci Rev., 60*, 503-530, 1992.

Ip, W. -H., D. J. Williams, R. W. McEntire, B. Mauk, Energetic ion sputtering effects at Ganymede, *Geophys. Res. Lett., 24*, 2631-2634, 1997.

Johnson, R. E., Polar 'caps' on Ganymede and Io revisited, *Icarus, 128*, 469-471, 1997.

Johnson, R. E., Sputtering and desorption from icy surfaces, in *Solar System Ices*, edited by B. Schmitt et al., pp. 303-334, Kluwer Acad., Norwell, Mass., 1998.

Johnson, R. E., and W. A. Jesser, O_2/O_3 microatmospheres in the surface of Ganymede, *Astrophys. J., 480*, L79-L82, 1997.

Johnson, R. E and T. I. Quickenden, Photolysis and radiolysis of water ice on outer solar system bodies, *J. Geophys Res., 102*, 10,985–10,996, 1997.

Kivelson, M G., K. K. Khurana, C. T. Russell, R. J. Walker, J. Warnecke, F. V. Coroniti, C. Polanskey, D. J. Southwood, and G. Schubert, Discovery of Ganymede's magnetic field by the Galileo spacecraft, *Nature, 384*, 537-541, 1996.

Lane, A. L., R. M. Nelson, and D. L. Matson, Evidence for sulphur implantation in Europa's UV absorption band, *Nature, 292*, 38-39, 1981.

Millis, R. L., and D. T. Thompson, UBV photometry of the Galilean satellites, *Icarus, 26*, 408-419, 1975.

Nelson, R. M., A. L. Lane, D. L. Matson, G J. Veeder, B. J. Buratti, and E. F. Tedesco, Spectral geometric albedos of the Galilean satellites from 0.24 to 0.34 micrometers: Observations with the International Ultraviolet Explorer, *Icarus, 72*, 358-380, 1987.

Noll, K. S., H. A. Weaver, and A. M. Gonnella, The albedo spectrum of Europa from 2200 Å to 3300 Å, *J. Geophys. Res., 100*, 19,057–19,059, 1995.

Noll, K. S., R. E. Johnson, A. L. Lane, D. L. Domingue, and H. A. Weaver, Detection of ozone on Ganymede, *Science, 273*, 341-343, 1996.

Pappalardo, R. T., et al., the Galileo Magnetometer Team, A comparison of the plasma bombardment boundary on Ganymede's surface to Galileo imaging data (abstract), *Bull. Am. Astron Soc.*, 30, 1120, 1998.

Pospieszalska, M. K. and R. E. Johnson, Magnetospheric ion bombardment profiles of satellites: Europa and Dione, *Icarus, 78*, 1-13, 1989.

Purves, N. G., and C. B. Pilcher, Thermal migration of water on the Galilean satellites, *Icarus, 43*, 51-55, 1980.

Reimann, C. T., J. W. Boring, R. E. Johnson, J. W. Garrett, and K. R. Farmer, Ion-induced molecular ejection from D_2O ice, *Surf. Sci., 147*, 227-240, 1984.

Rottman, G. J , T. N. Woods, and T. P. Sparn, Solar-Stellar Irradiance Comparison Experiment 1 1. Instrument design and operation, *J. Geophys. Res., 98*, 10,667-10,677, 1993.

Sieveka, E. M., and R. E. Johnson, Thermal- and plasma-induced molecular redistribution on the icy satellites, *Icarus, 51*, 528-548, 1982.

Smith, B. A., et al., The Galilean satellites and Jupiter. Voyager 2 imaging science results, *Science, 206*, 927-950, 1979

Spencer, J. R., W. M. Calvin, and M. J. Person, Charge-coupled device spectra of the Galilean satellites: Molecular oxygen on Ganymede, *J. Geophys. Res , 100*, 19,049-19,056, 1995.

Vaida, V., D. J. Donaldson, S. J. Strickler, S. L. Stephens, and J. W. Birks, A reinvestigation of the electronic spectra of ozone: Condensed-phase effects, *J. Phys. Chem , 93*, 506-508, 1989.

Vidal, R. A., D. Bahr, R. A. Baragiola, M Peters, Oxygen on Ganymede: Laboratory studies, *Science, 276*, 1839-1842, 1997.

C.A. Barth, A.R. Hendrix, and C.W. Hord, Laboratory for Atmospheric and Space Physics, Campus Box 590, University of Colorado, Boulder, CO 80309-0590. (hendrix@colorado edu)

(Received September 28, 1998; revised January 8, 1999; accepted January 22, 1999)